

2.23 GHz gating InGaAs/InP single-photon avalanche diode for quantum key distribution

Jun Zhang^{*a}, Patrick Eraerds^a, Nino Walenta^a, Claudio Barreiro^a, Rob Thew^a, and Hugo Zbinden^a

^aGroup of Applied Physics, University of Geneva, 1211 Geneva 4, Switzerland

ABSTRACT

We implement an InGaAs/InP single-photon avalanche diode (SPAD) for single-photon detection with the fastest gating frequency reported so far, of 2.23 GHz, which approaches the limit given by the bandwidth of the SPAD - 2.5 GHz. We propose a useful way to characterize the afterpulsing distribution for rapid gating that allows for easy comparison with conventional gating regimes. We compare the performance of this rapid gating scheme with free-running detector and superconducting single-photon detector (SSPD) for the coherent one-way quantum key distribution (QKD) protocol. The rapid gating system is well suited for both high-rate and long-distance QKD applications, in which Mbps key rates can be achieved for distances less than 40 km with 50 ns deadtime and the maximum distance is limited to ~ 190 km with $5 \mu\text{s}$ deadtime. These results illustrate that the afterpulsing is no longer a limiting factor for QKD.

Keywords: single-photon avalanche diode, avalanche photodiode, single-photon detection, photon counting, rapid gating, quantum cryptography

1. INTRODUCTION

Near-infrared single-photon detection is one of the key components for diverse applications, e.g., quantum key distribution (QKD)¹ or optical time domain reflectometry.² InGaAs/InP SPADs working in the Geiger mode can provide a practical and reliable solution.^{3,4} The quenching electronics⁵ operating on these devices has been extensively investigated for more than two decades and has provided the most significant performance improvements. The avalanche amplitude is highly dependent on the excess bias voltage and the duration of the avalanche.⁷ Larger amplitudes are easier to discriminate, but more carriers are trapped by the defects in the multiplication layer.⁴ These carriers can be subsequently released and create undesired avalanches, called afterpulses. The population of trapped carriers exponentially decays in time, and increasing temperatures can accelerate the depopulation process and hence decrease the afterpulsing. Generally, the afterpulsing effect is the most limiting factor for SPAD performance. Apart from increasing deadtime or heating the diode, there are other approaches to decrease the afterpulsing, e.g., speeding up the quenching time by integrating the quenching electronics into a single chip,^{6,7} or utilizing rapid gating with ultrashort gating durations.⁸⁻¹²

In general, in rapid gating systems, the gating repetition frequency (f_g) can reach the GHz level and the effective gating width (t_g) is usually below 300 ps. Therefore, the number of carriers created during an avalanche and thus the afterpulsing is significantly reduced but at the same time the avalanche amplitude becomes quite small, i.e., a few mV in general.⁸⁻¹² The essence of rapid gating is to then extract faint avalanches while maintaining a sufficient signal-noise ratio (SNR) between avalanche signals and capacitive response signals. So far, there are two methods to implement rapid gating, i.e., sine wave gating and filtering,^{8,9} self-differencing^{10,11} as well as a hybrid approach combining the above techniques.¹² For high-speed synchronous single-photon detection, f_g is a crucial parameter. Firstly, the value of f_g determines the operation speed of the whole system in applications. Secondly, increasing f_g correspondingly decreases t_g and thus the afterpulsing, for a fixed excess bias (V_e). Most InGaAs/InP SPADs used for single-photon detection were originally designed for 2.5 Gbps

Further author information: (Send correspondence to Jun Zhang)

E-mail: Jun.Zhang@unige.ch; Telephone: +41 (0)22 379 68 82; Fax: +41 (0)22 379 39 80

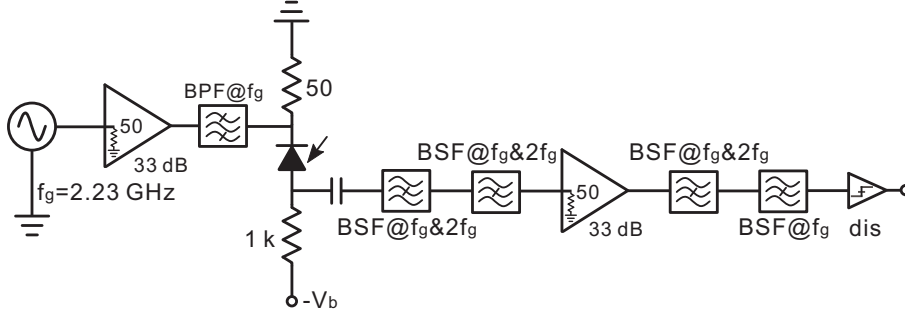


Figure 1. The experimental setup. BPF: band-pass filter; BSF: band-stop filter; f_g : gating frequency; dis: discriminator; $-V_b$: negative dc bias; @: the center frequency.

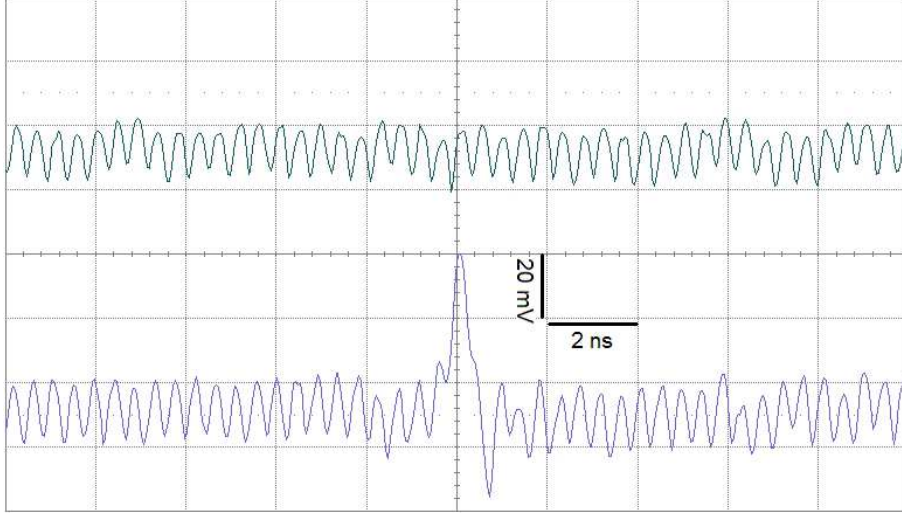


Figure 2. Typical capacitive response signal without avalanche (top) and avalanche signal (bottom) observed on oscilloscope after four BSFs and the amplifier. The horizontal and vertical units are 2 ns/division and 20 mV/division, respectively.

classical optical communication. Considering the frequency response limits of these photodiodes and the final SNRs, the limit of f_g for rapid gating could be presumed to be around 2.5 GHz.

In this Letter we report a rapid gating scheme with $f_g=2.23$ GHz that approaches the above mentioned frequency limit with detection efficiencies over 10%. We also illustrate a simple method to characterize the afterpulsing distribution in time that allows for easy comparison with conventional gating SPADs. Finally, we simulate the performance difference between rapid gating and free-running SPADs for QKD applications.

2. THE EXPERIMENT

The entire detection scheme is depicted in Figure 1. In our experiment, we employ the method of sine gating and filtering. The original sine wave signals from the generator (Agilent E4433B) pass through a 33 dB amplifier (Mini-Circuits ZHL-42W) and a band-pass filter (BPF) to produce gates with peak-peak amplitude (V_{pp}) of ~ 7.5 V. The output signals from the SPAD are processed by four band-stop filters (BSFs) and another 33 dB amplifier to extract the avalanche signals. The BSFs suppress the capacitive response signals induced by the SPAD at the fundamental frequency f_g and also the second harmonic $2f_g$. All the BSFs and the BPF are designed and fabricated using microstrips (FR4 substrate, dielectric constant $\epsilon=4.5$, height $H=1.43$ mm, thickness $T=35$ μm , and $Z_{in}=Z_{out}\equiv 50\Omega$). The final response and avalanche signals in front of the discriminator (dis) are captured by an oscilloscope (LeCroy WaveMaster 8600A, 6 GHz bandwidth and 20 GS/s), see Figure 2. We can deduce that the typical amplitudes of response and avalanche signals without the amplifier should be ~ 0.5 mV and 1 mV, respectively. The avalanche amplitude depends on many factors such as the actual gating duration, the excess bias V_e , the variation of the multiplication gain, the absorbed photon number and so on.

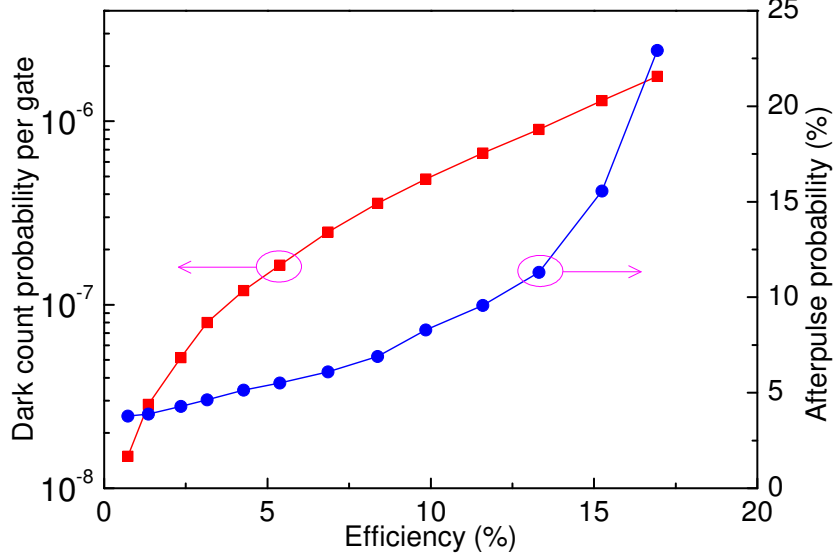


Figure 3. Plot of dark count probability per gate and afterpulse probability as a function of efficiency at $T=-40^{\circ}\text{C}$ and a mean photon number per laser pulse of 0.1.

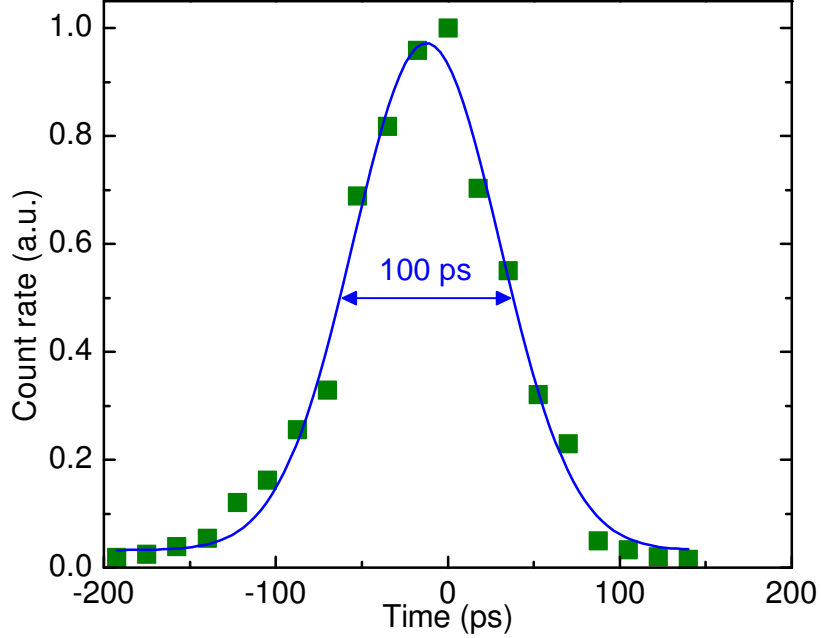


Figure 4. Count rate distribution obtained by delaying the position of the laser pulse with respect to the detection gate under the conditions of 10% efficiency and $T=-40^{\circ}\text{C}$. The effective gating width (t_g) is 100 ps.

3. RESULTS AND DISCUSSIONS

To characterize the performance of the system, we use the same SPAD (#1 SPAD) and the same calibration methods as used in Ref.¹² The 10 MHz synchronous output from the generator drives an ultrashort laser diode in the telecom regime (1550 nm) with ~ 30 ps width (PicoQuant PDL 800-B), which is attenuated down to the single-photon level per pulse. We apply a 10 ns “deadtime”¹² to the discriminator output, which means that once a detection is recorded all signals in the following 10 ns are ignored. The photon detections are counted by the coincidences between the laser pulses and the detections, while all the remaining detections are attributed

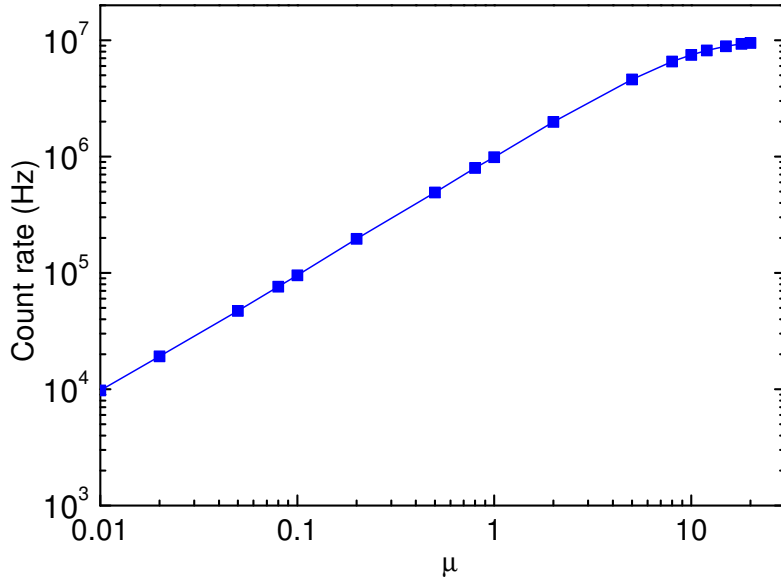


Figure 5. Count rates versus the mean photon number per laser pulse at 10 % efficiency. The saturated count rate reaches ~ 10 MHz, i.e., the laser frequency.

to dark counts and afterpulses. The calibrated results are shown in Figure 3. The efficiency η is calculated as¹²

$$\eta = \frac{1}{\mu} \cdot \ln \frac{1 - P_{dc}}{1 - P_{de}}, \quad (1)$$

where μ is the mean photon number per laser pulse, P_{dc} is the dark count probability per gate and P_{de} is the photon detection probability per laser pulse. When $\eta=10\%$, the afterpulse probability (P_{ap}) is 8.3% at $T=-40^\circ\text{C}$, equivalent to $\sim 4 \times 10^{-5} \text{ ns}^{-1}$ calculated according to Eqn. 3 in Ref.¹² P_{dc} is 4.8×10^{-7} per gate, equivalent to $4.8 \times 10^{-6} \text{ ns}^{-1}$ since $t_g=100 \text{ ps}$, see Figure 4. At a fixed excess bias V_e , the value of t_g depends on the sine gate amplitude V_{pp} . Larger V_{pp} corresponds to smaller t_g , which can suppress the afterpulsing effect but degrades the SNR and increases the processing difficulty for the back-end electronics.

Let us compare the normalized parameters of the SPAD to the results in Ref.,¹² where at $f_g=921 \text{ MHz}$, $T=-30^\circ\text{C}$ and $\eta=9.3\%$, P_{dc} per ns ($P_{dc}[\text{ns}^{-1}]$) and P_{ap} per ns ($P_{ap}[\text{ns}^{-1}]$) are $2.8 \times 10^{-6} \text{ ns}^{-1}$ and $1.6 \times 10^{-4} \text{ ns}^{-1}$.¹² The values of $P_{dc}[\text{ns}^{-1}]$ are at the same levels and the small difference is probably due to the V_{pp} difference. $P_{ap}[\text{ns}^{-1}]$ in our experiment with even cooler temperature is only 1/4 of the value in Ref.¹² The main reason for the improvement is attributed to the smaller t_g .

Figure 5 illustrates the count rate characteristic as a function of mean photon number per laser pulse. As μ rises the count rate linearly increases when $\mu < 10$, and finally the count rate is saturated to ~ 10 MHz, which is the same as the laser frequency. Since this frequency was fixed inside the generator and the maximum laser driver frequency was also limited, we could not test the theoretically maximum count rate of SPAD, i.e., ~ 100 MHz given by the 10 ns “deadtime” setting.

We also use the coincidence method¹² to characterize the afterpulsing distribution in a $1 \mu\text{s}$ range, see Figure 6. The laser repetition frequency is as low as 500 kHz and the coincidence window is 50 ns. The result is shown in the histogram of Figure 6, in which the constant dark count contribution has been subtracted. $P_{ap}[\text{ns}^{-1}]$ is also shown in the right axis of Figure 6 and calculated as

$$P_{ap}[\text{ns}] = \frac{P_{ap}}{50 \cdot t_g \cdot f_g}, \quad (2)$$

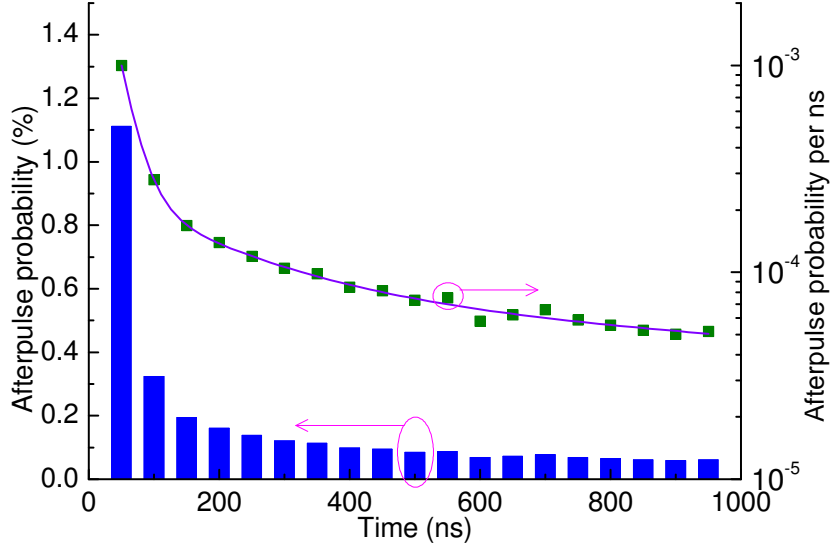


Figure 6. The afterpulsing distribution in a $1\ \mu\text{s}$ range with a laser pulse frequency of 500 kHz at 10% efficiency and $T=-40\ ^\circ\text{C}$. The histogram (left axis) is measured by scanning the position of a 50 ns coincidence window. The corresponding normalized parameter $P_{ap}[\text{ns}^{-1}]$ (right axis) is plotted and fitted.

where $t_g \cdot f_g$ is the duty cycle and at each bin the minor afterpulsing contribution from the previous bins is corrected through the iterative calculations. The curve is fitted using a multiple detrapping model,⁷ which suggests that there are mainly two kinds of detrapping types with a quite short lifetime of $\sim 100\ \text{ns}$ and a relatively long lifetime of $> 1\ \mu\text{s}$. In Figure 6, $P_{ap}[\text{ns}^{-1}]$ reaches $5 \times 10^{-5}\ \text{ns}^{-1}$, equivalent to $10 \cdot P_{dc}[\text{ns}^{-1}]$, at the time of 900 ns. For comparison, in the case of integrated active quenching system,⁷ the typical value with the same temperature and time settings is $7 \times 10^{-3}\ \text{ns}^{-1}$, equivalent to $2058 \cdot P_{dc}[\text{ns}^{-1}]$ ($P_{dc}[\text{ns}^{-1}] = 3.4 \times 10^{-6}\ \text{ns}^{-1}$), and a deadtime setting $> 20\ \mu\text{s}$ is required to suppress $P_{ap}[\text{ns}^{-1}]$ down to $5 \times 10^{-5}\ \text{ns}^{-1}$, equivalent to $14.7 \cdot P_{dc}[\text{ns}^{-1}]$, see Figure 8(b) in Ref.⁷

4. QKD SIMULATIONS

Rapid gating detection would appear to be well suited to high-speed QKD applications.^{13,14} To look more closely at this, we model and simulate the secure key rate for the coherent one-way (COW) QKD¹⁵ scheme, as a function of distance, based on our rapid gating and free-running SPADs^{6,7} as well as SSPDs,¹⁶ see Figure 7. The typical parameters of the QKD system for modeling such as mean photon number per pulse, decoy pulse probability, insertion loss for Bob's system, interferometric visibility etc., are taken from Ref.¹⁵ The typical parameter values of the rapid gating and free-running SPADs at 10% efficiency are taken from this experiment and Ref.,¹⁵ respectively. For a fair comparison, the parameters of the SSPD are assumed as follows, 10% system detection efficiency, 10 Hz dark count rate and minimum pulse width of 20 ns, corresponding to maximum count rate of 50 MHz. These SSPD parameters are probably not the best results reported so far, but they are not necessarily underestimated. For instance, the system detection efficiency of the SSPD in our group is 2.6% with 10 Hz dark count rate.¹⁸ We also assume that the detection window is 100 ps for all the three kinds of detectors.

In the rapid gating case, the crucial parameter, the afterpulse probability is estimated as

$$\overline{P_{ap}} = \int_{\tau_d}^{\overline{\Delta T}} f(t) dt, \quad (3)$$

where $\overline{P_{ap}}$ is the average afterpulse probability, τ_d is the deadtime, $\overline{\Delta T}$ ($> \tau_d$) is the average time interval between two detections, and $f(t)$ is the above mentioned fitting function in Figure 6. We focus on two extreme regimes: short distances with high rates and maximum distances.

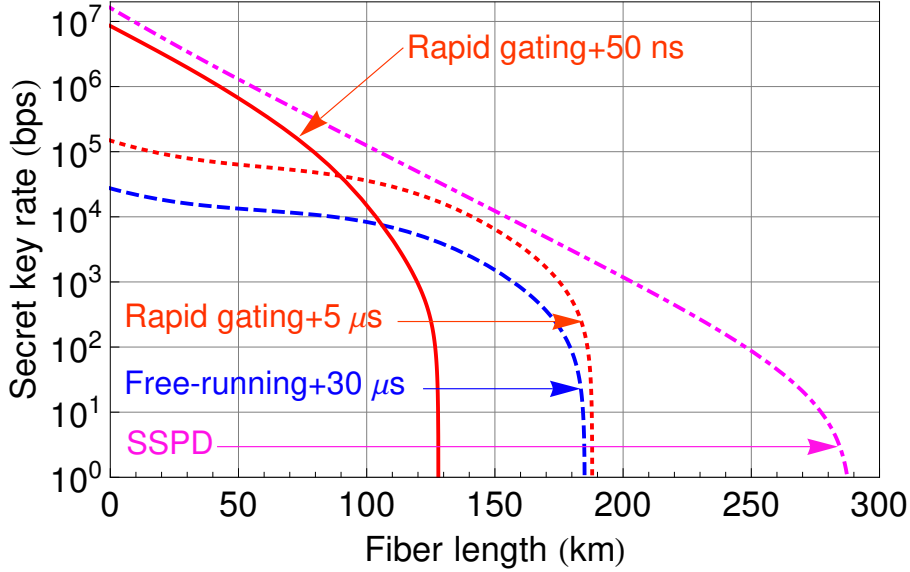


Figure 7. The simulation of secure key rate for the COW QKD protocol versus fiber distance, using the rapid gating SPAD with 50 ns (solid) and 5 μ s (dotted) deadtime and the free-running SPAD^{6,7} with 30 μ s deadtime (dashed), as well as SSPD (dot-dashed), respectively.

Firstly, let us look at short distances. The rapid gating scheme with $\tau_d=50$ ns provides considerably high rates over short distances, e.g., Mbps key rates for distances less than 40 km. This results are much better than the free-running SPAD and approach the results of SSPD, which implies that the rapid gating SPAD with small τ_d is well suited in short distance regimes.

Secondly, the maximum distance in this case is limited to ~ 130 km. However, if τ_d is increased, the maximum distance can be increased accordingly because for longer distances the probability of a photon arriving is significantly reduced and hence we can increase τ_d to suppress the afterpulsing without adversely affecting the rates. When $\tau_d=5$ μ s, the key rates are reduced for short distances compared to $\tau_d=50$ ns but the maximum distance is extended up to ~ 190 km, see the dotted line in Figure 7. Moreover, we find that we approach the distance limit for the ideal case with the assumption of no afterpulsing, which implies that the afterpulse probability of rapid gating SPAD can be suppressed down to approximately zero with $\tau_d=5$ μ s. Interestingly, the free-running SPAD with $\tau_d=30$ μ s can implement almost the same maximum distance, probably because $\tau_d=30$ μ s is sufficient to suppress the afterpulse probability of free-running SPAD down to a negligible level and therefore the maximum distance is only limited by the dark count characteristics.

Finally, we model the system with SSPD for comparison, see the dot-dashed line in Figure 7. We see that for short distances, SSPDs have only a minimal advantage over rapid gating SPADs in terms of rate. Nevertheless, the maximum distance that SSPDs can obtain is more than 280 km, due to the ultralow noise characteristics of such detectors. This suggests that SSPDs are well suited for ultra-long distance (>200 km) applications, which was already verified by some previous experiments.¹⁷⁻¹⁹ The maximum distance difference between the rapid gating SPADs and the SSPDs is essentially due to the difference in dark count characteristics. For instance, the dark count rate of our rapid gating SPAD is 480 times higher than that of SSPD. There is still some room to optimize the rapid gating SPAD, e.g., cooling down further the temperature of the SPAD while increasing the deadtime setting. However, short distances with high key rates are more interesting than ultra-long distances with ultralow key rates for practical applications.

In general, we can conclude that the afterpulsing is no longer a limiting factor for QKD. For high-rate QKD applications, rapid gating SPADs with small τ_d are favorable candidates. Both free-running and rapid gating SPADs are well suited for long-distance applications, say, <200 km, while SSPDs remain advantageous for distances >200 km. In practice, rapid gating SPADs are definitely the appropriate choice compared to SSPDs, due to the disadvantages of SSPDs such as cryogenic requirements and non-cost-effectiveness.

5. CONCLUSIONS

In conclusion, we demonstrate a near-infrared single-photon detector, based on an InGaAs/InP SPAD, capable of synchronized operation at 2.23 GHz clock rates. This scheme can effectively suppress the afterpulsing. We illustrate a useful technique to characterize the afterpulsing distribution for easy comparison between different systems. We also demonstrate the performance impact of these types of devices on QKD. Rapid gating SPADs are well suited to both high-rate and long-distance QKD applications, and modeling suggests that the maximum distances can reach ~ 190 km. Most importantly, we conclude that the afterpulsing is no longer a limiting factor for QKD. Finally, dark count remains the most of important bottleneck for further increases in the maximum achievable distances. Suppressing dark count rates of SPADs is still an open issue that deserves investigation to further extend QKD distances with practical detection schemes.

ACKNOWLEDGMENTS

The authors thank O. Guinnard and N. Gisin for useful discussions and acknowledge financial support from the Swiss NCCR-Quantum Photonics.

REFERENCES

- [1] Gisin, N., Ribordy, G., Tittel, W. and Zbinden, H., “Quantum cryptography,” *Rev. Mod. Phys.* 74, 145 (2002).
- [2] Eraerds, P., Legre, M., Zhang, J., Zbinden, H. and Gisin, N., “Photon Counting OTDR: Advantages and Limitations,” arXiv:1001.0694v2.
- [3] Ribordy, G., Gautier, J.D., Zbinden, H. and Gisin, N., “Performance of InGaAs/InP Avalanche Photodiodes as Gated-Mode Photon Counters,” *Appl. Opt.* 37, 2272 (1998).
- [4] Itzler, M. A., Ben-Michael, R., Hsu, C.-F., Slomkowski, K., Tosi, A., Cova, S., Zappa, F. and Ispasoiu, R., “Single photon avalanche diodes (SPADs) for 1.5 μ m photon counting applications,” *J. Mod. Opt.* 54, 283 (2007).
- [5] Cova, S., Ghioni, M., Lacaíta, A., Samori, C. and Zappa, F., “Avalanche photodiodes and quenching circuits for single-photon detection,” *Appl. Opt.* 35, 1956 (1996).
- [6] Thew, R. T., Stucki, D., Gautier, J.-D., Zbinden, H. and A. Rochas, “Free-running InGaAs/InP avalanche photodiode with active quenching for single photon counting at telecom wavelengths,” *Appl. Phys. Lett.* 91, 201114 (2007).
- [7] Zhang, J., Thew, R., Gautier, J.-D., Gisin, N. and Zbinden, H., “Comprehensive Characterization of InGaAs/InP Avalanche Photodiodes at 1550 nm With an Active Quenching ASIC,” *IEEE J. Quantum Electron.* 45, 792 (2009).
- [8] Namekata, N., Sasamori, S. and Inoue, S., “800 MHz single-photon detection at 1550-nm using an InGaAs/InP avalanche photodiode operated with a sine wave gating,” *Opt. Express* 14, 10043 (2006).
- [9] Namekata, N., Adachi, S. and Inoue, S., “1.5 GHz single-photon detection at telecommunication wavelengths using sinusoidally gated InGaAs/InP avalanche photodiode,” *Opt. Express* 17, 6275 (2009).
- [10] Yuan, Z. L., Kardynal, B. E., Sharpe, A. W. and Shields, A. J., “High speed single photon detection in the near infrared,” *Appl. Phys. Lett.* 91, 041114 (2007).
- [11] Dixon, A. R., Dynes, J. F., Yuan, Z. L., Sharpe, A. W., Bennett, A. J. and Shields, A. J., “Ultrashort dead time of photon-counting InGaAs avalanche photodiodes,” *Appl. Phys. Lett.* 94, 231113 (2009).
- [12] Zhang, J., Thew, R., Barreiro, C. and Zbinden, H., “Practical fast gate rate InGaAs/InP single-photon avalanche photodiodes,” *Appl. Phys. Lett.* 95, 091103 (2009).
- [13] Namekata, N., Fujii, G., Inoue, S., Honjo, T. and Takesue, H., “Differential phase shift quantum key distribution using single-photon detectors based on a sinusoidally gated InGaAs/InP avalanche photodiode,” *Appl. Phys. Lett.* 91, 011112 (2007).
- [14] Dixon, A. R., Yuan, Z. L., Dynes, J. F., Sharpe, A. W. and Shields, A. J., “Gigahertz decoy quantum key distribution with 1 Mbit/s secure key rate,” *Opt. Express* 16, 18790 (2008).

- [15] Stucki, D., Barreiro, C., Fasel, S., Gautier, J., Gay, O., Gisin, N., Thew, R., Thoma, Y., Trinkler, P., Vannel, F. and Zbinden, H., "Continuous high speed coherent one-way quantum key distribution," *Opt. Express* 17, 13326 (2009).
- [16] Gol'tsman, G. N., Okunev, O., Chulkova, G., Lipatov, A., Semenov, A., Smirnov, K., Voronov, B., Dzardanov, A., Williams, C. and Sobolewski, R., "Picosecond superconducting single-photon optical detector," *Appl. Phys. Lett.* 79, 705 (2001).
- [17] Takesue, H., Nam, S. W., Zhang, Q., Hadfield, R. H., Honjo, T., Tamaki, K. and Yamamoto, Y., "Quantum key distribution over a 40-dB channel loss using superconducting single-photon detectors," *Nat. Photonics* 1, 343 (2007).
- [18] Stucki, D., Walenta, N., Vannel, F., Thew, R. T., Gisin, N., Zbinden, H., Gray, S., Towery, C. R. and Ten, S., "High rate, long-distance quantum key distribution over 250 km of ultra low loss fibres," *New Journal of Physics* 11, 075003 (2009).
- [19] Chen, T. Y., Wang, J., Liu, Y., Cai, W. Q., Wan, X., Chen, L. K., Wang, J. H., Liu, S. B., Liang, H., Yang, L., Peng, C. Z., Chen, Z. B. and Pan, J. W., "200 km Decoy-state quantum key distribution with photon polarization," arXiv:0908.4063v1.